

A novel way to monitor the sequential destruction of parent-daughter crystals in isotactic polypropylene under uniaxial tension

Yanping Liu · Zhihua Hong · Liangui Bai ·
Nan Tian · Zhe Ma · Xiangyang Li ·
Liang Chen · Benjamin S. Hsiao · Liangbin Li

Received: 5 November 2013 / Accepted: 23 December 2013 / Published online: 22 January 2014
© Springer Science+Business Media New York 2014

Abstract The cross-hatched structural evolution of isotactic polypropylene (iPP) during uniaxial tensile deformation was investigated with in situ synchrotron radiation wide angle X-ray scattering. An effective way was developed to study parent and daughter lamellae separately with in situ environment. iPP sample was preoriented to generate a bimodal orientation of lamellae for distinguishing the parent and daughter lamellae, which will orient in orthogonal directions under flow-induced crystallization. The dumbbell samples were prepared along different angles with respect to preorientation direction to achieve multisided stretching. The structural evolution of parent and daughter lamellae was followed by recording the scattering from (110) crystallographic plane. It was observed that the parent lamellae were destroyed earlier than daughter ones, no matter which the tensile direction was. Mesophase was observed at very small strain of 0.3, immediately after the damage of cross-hatched structure, which may be attributed to the destruction of parent lamellae. Deformation induced mesophase was proved to

be the small crystal cluster which was transformed from parent and daughter lamellae.

Introduction

Isotactic polypropylene (iPP) is one of the most important thermoplastic polymers, owing to its lower manufacturing cost and rather versatile properties. It has gained extensive study not only for the commercial value, but also for scientific interests [1, 2]. iPP is well known for the typical polymorphic structure with four main crystal forms: monoclinic α -modification, hexagonal β -modification, triclinic γ -modification, and smectic phase [3–11]. In the α -modification of iPP, there is a characteristic lamellar branching known as the cross-hatched structure, which has no counterpart in other semicrystalline polymers [12]. The cross-hatched structure was first noticed as the tightly woven habit in the spherulitic crystallization in iPP [2]. Then, Khoury [13] found the intercross branching with an acute angle of 80° existed in solution-grown dendrites. Moreover, he proposed the epitaxial deposition of branches with their a and c axes parallel to the c and a axes of parent lamellae. The work on the thin films of iPP by Padden and Keith [14] confirmed Khoury's findings in melt-grown crystal and the intersection angle was more accurately determined to $80^\circ 40'$ using diffraction data. Later, more researcher developed this structure model and proposed the molecular origin of the cross-hatched structure [15–17]. However, the cross-hatched structure, which is constituted by the parent and daughter lamellae, has not been studied separately with in situ environments.

The cross-hatched structure is known to have influence on important material performances such as fatigue life [18], resistance to deformation [19], and surface properties such

Y. Liu · Z. Hong · L. Bai · N. Tian · X. Li · L. Chen ·
L. Li (✉)
National Synchrotron Radiation Lab and College of Nuclear
Science and Technology, CAS Key Laboratory of Soft Matter
Chemistry, University of Science and Technology of China,
Hefei, China
e-mail: lbli@ustc.edu.cn

Z. Ma
Materials Technology, Eindhoven University of Technology,
Eindhoven, The Netherlands

B. S. Hsiao
Department of Chemistry, Stony Brook University, Stony Brook,
NY, USA

as wear and adhesion [20]. In the work on the deformation behavior of polymer material, it was found the brittle fracture [21, 22] in the specific case of iPP did not comply with the fibril formation at high strain in the conventional viewpoint [23–28]. The difference is attributed to restricted mobility of amorphous chain segments interlocked in regions between parent and daughter lamellae, which is a typical morphological feature of conventionally crystallized iPP [22, 29]. Thus, a greater understanding of the relationship between cross-hatched structure and macroscopic properties of iPP may allow tailored microstructures to be produced, extending the range of properties available for industrial applications. As hierarchically-structural material, the structural evolution induced by deformation in iPP has well been established at different scales [30–32]. Hay and Keller [32] observed the homogeneous and heterogeneous deformation behavior of micro-scale spherulites. Zuo et al. [33] proposed that the tie chain from interlamellar chain entanglement initiated the fragmentation of lamellar crystals under deformation, forming oriented mesophase. Based on in situ microbeam SAXS-WAXS-POM measurements, Nozue et al. [34] observed the evolution of cross-hatched structure during the hot drawing of spherulite and obtained the structural information of parent and daughter lamellae in various orientations. However, there is still a lack of systematic study on the deformation behavior focusing on the cross-hatched structure.

The most important issue in the study of cross-hatched structure lies on separate parent and daughter lamellae with in situ environment. In this study, in situ WAXS measurements are performed to monitor the structure evolution of parent and daughter lamellae during uniaxial tensile deformation from different directions. For the purpose to distinguish parent and daughter lamellae, we develop the oriented iPP film with extrusion and predrawn. To reduce the impact of prestretching, the samples were annealed at high temperature, and a nucleating agent DMDBS (1,3:24-bis (3,4-dimethylbenzylideno) sorbitol) was used to keep the orientation. Then, the samples were cut into dumbbell shape along different directions to achieve multisided tensile test, as stretching is along horizontal direction. For conciseness, L_m and L_d are used to represent parent and daughter lamellae, respectively. This method provides the chance to monitor the evolution of L_m and L_d during deformation separately.

Experiments

Materials

The iPP used in this study is a commercial product of Lanzhou petroleum chemical Co. (China), labeled F401,

which has M_w and M_n of about 530 and 160 kg/mol respectively. DMDBS, a nucleating agent for iPP, was kindly supplied from Milliken, was dried under vacuum for 24 h before mixing.

Sample preparation

iPP was compounded with DMDBS (0.5 wt%) in a corotating twin screw extruder at 225 °C. After extruding through a slit die, iPP was further stretched to a draw ratio of about eight to obtain highly oriented samples.

To obtain isothermal crystallized samples, the extruded samples were first heated up to 190 °C and kept for 30 min in a vacuum oven to prevent degradation. At this temperature, iPP melted while the nucleation agent DMDBS did not melt, which maintained the orientation induced by the predrawing. Then, the samples were transferred to another vacuum oven where the temperature was preset at 135 °C. Isothermal crystallization at 135 °C took about 40 min. The crystallization kinetics was studied with WAXS, which confirmed that 40 min was enough for complete crystallization. The obtained samples were highly oriented, because the orientation of DMDBS was kept during melting. As shown in Fig. 1, the samples were cut into dumbbell shape with lengthwise direction lying between 0° and 90° with respect to the drawing direction for tensile test.

Tensile test

The dumbbell shaped samples were mounted between two clamps of a homemade miniature tensile tester. The drawing speed was 0.58 μm/s. Uniaxial tensile tests were performed at room temperature. The in situ synchrotron radiation wide angle X-ray scattering (WAXS) were carried out during the whole process.

WAXS was carried out on the X-ray-scattering station with Mar 345 image plate (3070 × 3070 pixels with pixel size 150 μm) as a detector and with a wavelength of 0.154 nm in National Synchrotron Radiation Laboratory in Hefei (China). The sample-to-detector distance was calibrated to be 299 mm, and the data acquisition time for each frame was 60 s. Fit2D software from European Synchrotron Radiation Facility was used to analyze WAXS patterns [35].

Results

Figure 2 shows WAXS images for the selected three experiments in parallel (P), vertical (V), and tilt (T) directions. The angle between preorientation direction of L_m and the drawing direction are 0°, 88.7°, and 76° for P, V, and T experiments as shown in Fig. 1, respectively. Stretching is

Fig. 1 Schematic diagrams of the preparation for dumbbell samples in *P*, *V*, and *T* directions, with red dash arrows showing drawing directions. Preoriented cross-hatched structure is inserted. Letters *M* and *D* denote parent and daughter lamellae (Color figure online)

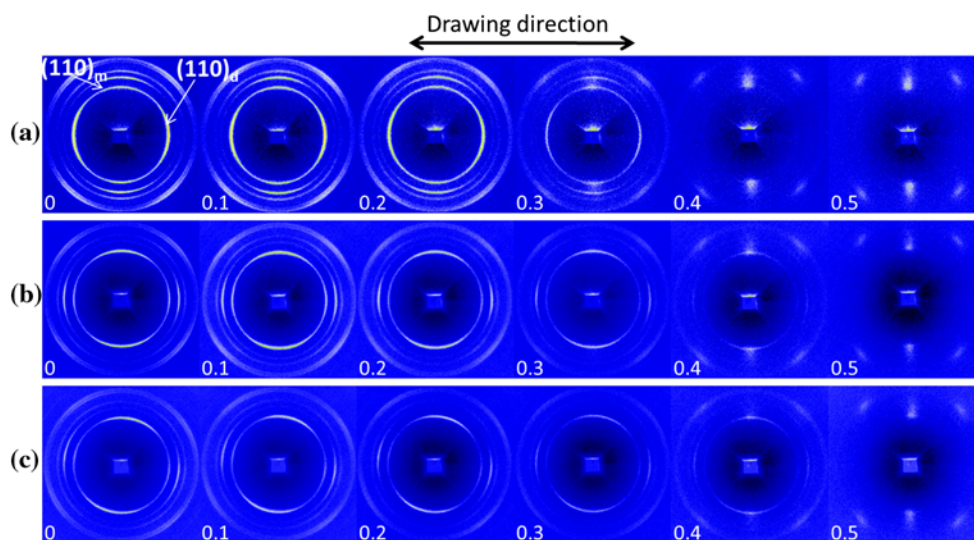
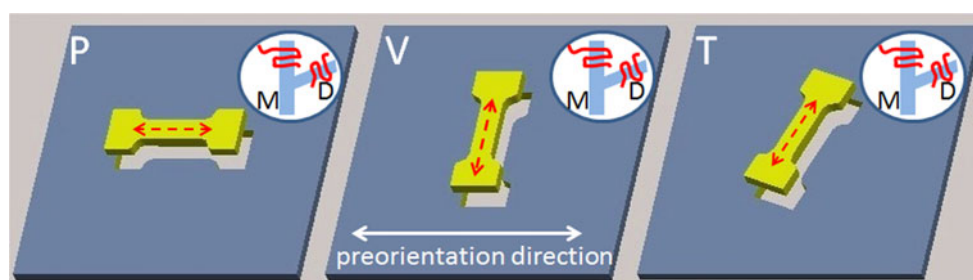


Fig. 2 Selected in situ WAXS images with strain inserted. **a–c** are corresponding to parallel, vertical, and tilt directions, respectively. The scattering arcs of (110) plane of L_m and L_d are indicated as $(110)_m$ and $(110)_d$, respectively

along horizontal direction in line with 0° . For the WAXS images before deformation (at strain of 0) in Fig. 2a which is *P* experiment, the (110) diffraction pattern is separated into six regions along with the azimuthal angle. The two diffraction arcs in meridian direction are from L_m while the other four arcs close to equator are diffracted from L_d . Oppositely, in *V* and *T* directions, the diffraction arcs for L_m and L_d locate in equator and meridian directions, respectively. Along with stretching, the diffraction arcs from both L_m and L_d become weaker and fade away. At the later stage of deformation, mesophase appears at such a small strain of 0.3 comparing with other works on the deformation-induced mesophase at room temperature [8, 10].

The quantitative analysis on the evolution of cross-hatched structure is displayed in Fig. 3, where the evolution of crystallinity and mesophase during deformation are presented. The corresponding engineering stress strain curves (ESSC) are also plotted in Fig. 3 for a direct correlation between structural evolution and mechanical properties. After yield point on the ESSC, collective lamellae slip starts, which leads to the decline of crystallinity. In the later stage of deformation, mesophase appears after the damage of cross-hatched structure under deformation. In

general, the destruction of crystal block is thought to be followed by the formation of fibrils [36]. However, the cross-hatched structure hinders the formation of fibril as mentioned above [22, 29], so mesophase appears at such a small strain. For detailed comparison, the modulus of elasticity and yield stress for three directions are displayed in Table 1. No obvious difference is observed, except for the strain softening which is the stress decreases with increasing deformation after yielding point [37]. When stress is applied from tilt direction, strain softening covers a wider strain region from 0.1 to 0.25 on the engineering stress–strain curve. The intrinsic strain softening is convincingly demonstrated to be influenced by thermal and mechanical histories, especially by means of preorientation [38]. As the samples underwent the same predeformation, the difference of macroscopic properties must come from the change of orientation directions. Either L_m or L_d is oriented along with the stretching direction in *P* and *V* experiments. However, crystal orientation is very weak in *T* experiment, so more work is needed for molecular reorientation and collective activity of slip motion [39].

Due to preorientation, the L_m and L_d can be distinguished as the scattering arcs especially for the crystallographic plane (110) locating in different directions. The

Fig. 3 The evolution of crystallinity and mesophase with respect to the corresponding engineering stress–strain curves for **a** P, **b** V, and **c** T directions

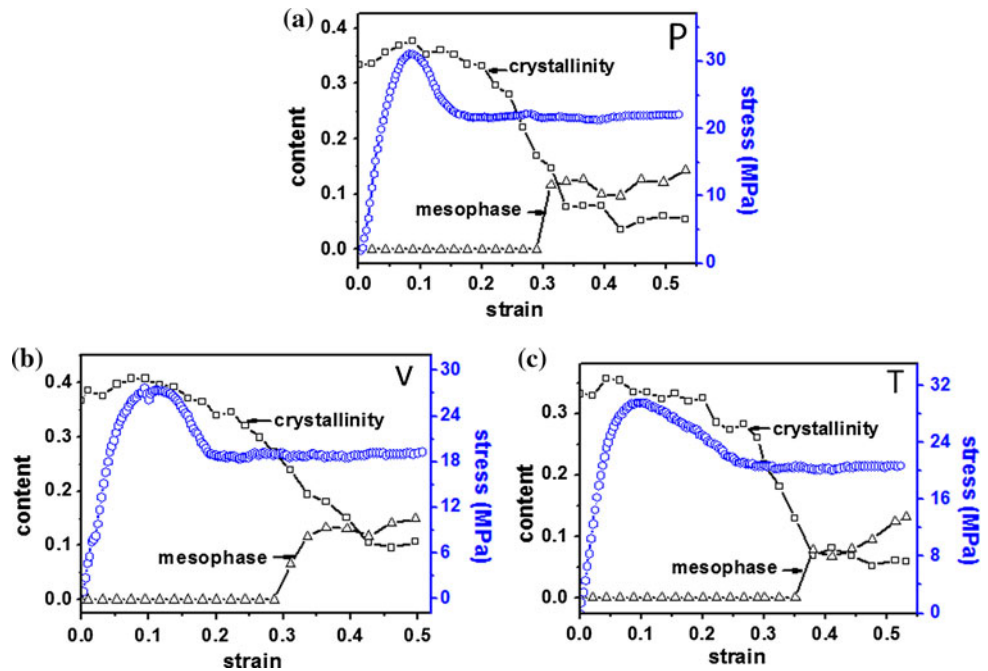


Table 1 The elasticity modulus and yield stress for three experiments

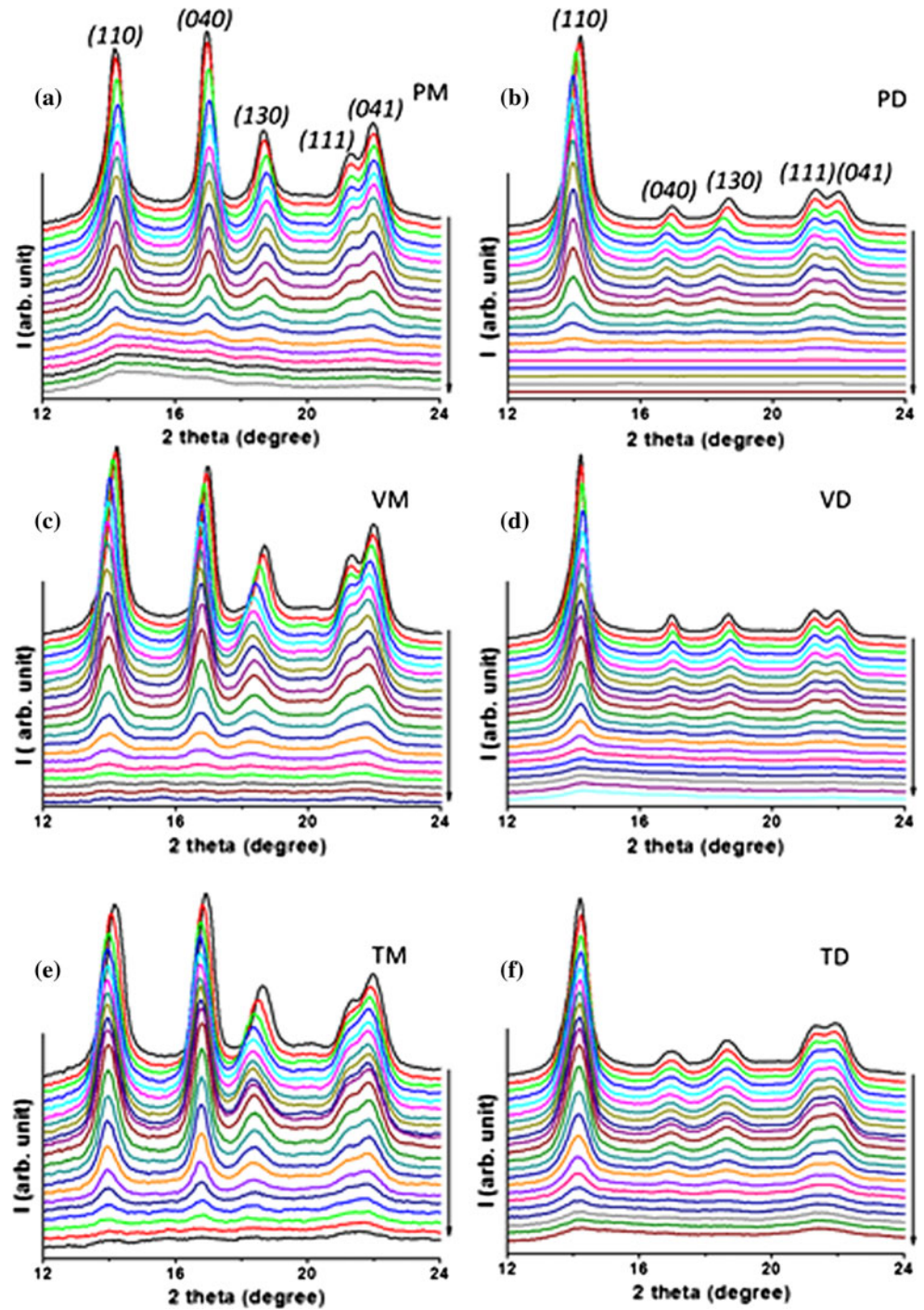
Item	P	V	T
Modulus (GPa)	0.428	0.417	0.518
Yield stress (MPa)	31.3	27.5	29.6

WAXS image can be divided into quadrants, with two of which covering the L_m scattering and the other two covering the L_d scattering. Therefore, the structural evolution can be followed from two directions, respectively. Thanks to the mask function of the Fit2D software, the one-dimensional (1D) WAXS intensity can be displayed for L_m and L_d separately in Fig. 4. The main diffraction peaks are observed at 2θ of about 14.2° , 16.9° , and 18.6° before stretching, which corresponds to crystallographic planes (110), (040), and (130), respectively. Figure 4a displays the 1D WAXS intensity for L_m , the peaks almost keep their positions during the deformation. It is important to notice that peak positions of (110) shift to small angle in the beginning of deformation and recover slightly with further stretching as shown in Fig. 4b, which is the scattering intensity from L_d in P experiment. Moreover, the similar shift happens to L_m in both V and T samples (Fig. 4c, e), while the peak positions of L_d keep unchanged (Fig. 4d, f). As the preorientations are different from each other, the biggest peak shift always happens to the lamellae with molecular orientation almost perpendicular to the drawing direction.

To compare the structural evolution between L_m and L_d , Fig. 5 displays the (110) d-spacing and the Full Width at Half Maximum (FWHM) of the (110) scattering intensity. For P experiment as shown in Fig. 5a, the (110) d-spacing of L_d increases from 0.623 to 0.635 nm sharply before yield strain, then declines slightly and almost keeps plateau. Meanwhile, different trend is found on the (110) d-spacing of L_m , which is a little decline before yielding and then increase. In contrast to the P direction, more obvious alternation happens to the L_m in V and T directions. As shown in Fig. 5b, c, there is a larger increase for (110) d-spacing of L_m before yield strain. After yielding, the recovery is faint in T direction comparing with V direction. In both directions, the (110) d-spacing of L_d does not change remarkably, which is also different from P direction. The FWHM of the scattering intensity is known to reflect the size of crystal. In Fig. 5a, before the strain of 0.3, there is only a small increase of FWHM for both L_m and L_d . A sharp jump of FWHM is observed near to the strain of 0.3, where the mesophase appears. Similarly, for vertical and tilt direction (Fig. 5b, c), the FWHM of L_m also increase abruptly at the strain where mesophase forms. However, the variation in the FWHM of L_d lags behind. It seems that there exists a relationship between the formation of mesophase and destruction of L_m .

According to Fig. 5a, the damage of L_m and L_d cannot be distinguished as both FWHMs rise up near to the strain of 0.3. Therefore, the azimuthal-integrated intensity of crystallographic plane (110) in P direction is plotted in Fig. 6a for further exploration. The scattering of L_m spreads around a peak position of 90° or 270° along the

Fig. 4 One-dimensional integrated WAXS curves for parent (M) and daughter (D) direction. The *top*, *middle*, and *bottom* rows are corresponding to *P*, *V*, and *T* directions, respectively



azimuthal angle, while the two peaks corresponding to L_d locate at about 6° and 172° in the azimuthal distribution. Along with stretching, the two broad scattering peaks of L_m shift slightly and transform into two sharply ones of mesophase. Meanwhile, the azimuthal angle of L_d does not show obvious shift, but broadens up in later stage. Obviously, the scattering from L_m disappears earlier than that from L_d . To deeply investigate the structure evolution

during deformation, the peak position and the corresponding FWHM' of L_m is displayed in Fig. 6b. The FWHM' is the full width at half maximum of azimuthal integrated intensity, which is different from FWHM as mentioned above. Only after yield strain (in zone II), there is a small peak shift from 270.5° to 267.3° due to lamellar rotation. In zone III where plastic deformation develops further, the FWHM's decline monotonously and the peak

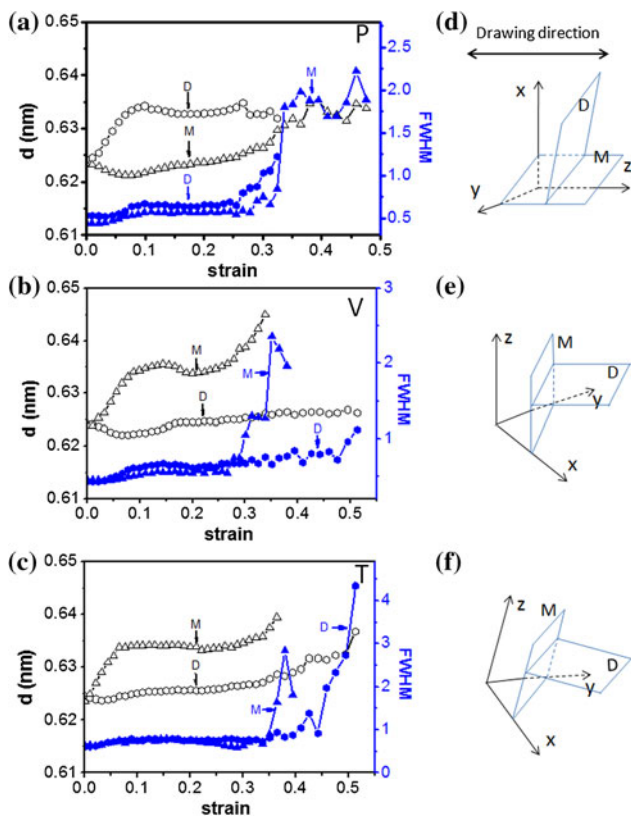


Fig. 5 a–c are the evolution of the interplanar spacing and the FWHM of the scattering intensity from (110). d–f are the corresponding force conditions of (110) crystallographic planes. Drawing direction is inserted in the figure. Circle and triangle are denoting daughter (D) and parent lamellae (M), respectively

position shifts back, because molecular chains reorient their interested axis to the drawing direction. At the strain where mesophase appears, it enters into zone IV, where massive destruction happens to the cross-hatched structure. Therefore, it shows a nice correlation between the deformation process of the cross-hatched structure and the mechanical property.

Similar analysis is also applied to V and T directions. As shown in Figs. 4 and 5, the scattering intensity from parent lamellae disappears or weakens when mesophase forms. Therefore, the azimuthal angle and FWHM' of (110)

scattering intensity from L_m only can be fit out until the strain where mesophase appears for these two directions. According to Fig. 7a, the L_m just rotates during the deformation, which leads to the shift of azimuthal angle. The orientation degree of L_m does not change too much as the FWHM' keeps stable almost. However, the azimuthal angle near to 90° and 270° can be fit in a wider strain region both for V and T directions, which is displayed in Fig. 7b. Comparing with V direction, the azimuthal angle of L_d shifts drastically in T direction, because the orientation of molecular chain in T direction deviates from drawing direction more gravely. Interestingly, the FWHM's of (110) scattering intensity from L_d for both directions show a similar trend of rising after yield strain and descending after strain softening. Because of lamellae slip in the beginning, the FWHM' increases first. When plastic deformation develops further, the molecular chains orient in the drawing direction, which leads to the decline of FWHM'.

Discussion

On the basis of in situ WAXS measurements during tensile deformation of preoriented iPP, two interesting findings can be extracted. (i) To preorient the cross-hatched structure is an effective method to study L_m and L_d separately with in situ environments. In this study, it is found that L_m are destroyed earlier than L_d , no matter what the force direction is. (ii) Different from previous study, mesophase appears at such a small strain in this study. Considering the strain when the cross-hatched structure is destroyed, it seems that mesophase is the small crystal cluster evolved from L_m and L_d . Focusing on these points, we will give some discussions in the following paragraphs.

Based on the study, it is deduced that L_m are destroyed before L_d . From the 2D-scattering patterns in Fig. 2, it is easy to find the (110) scattering from L_m disappear at the strain of 0.4 where that from L_d still exists, with the intensity weakens. This phenomenon is more obvious in V and T directions. For P experiment, the scattering from

Fig. 6 a The azimuthal-integrated intensity of (110) for P (parallel) direction. 0° is the horizontal direction. b Peak and FWHM' of parent crystal calculated from (a)

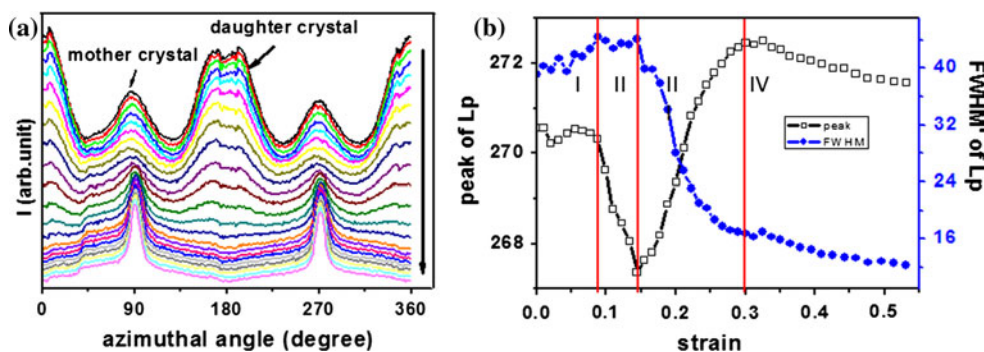
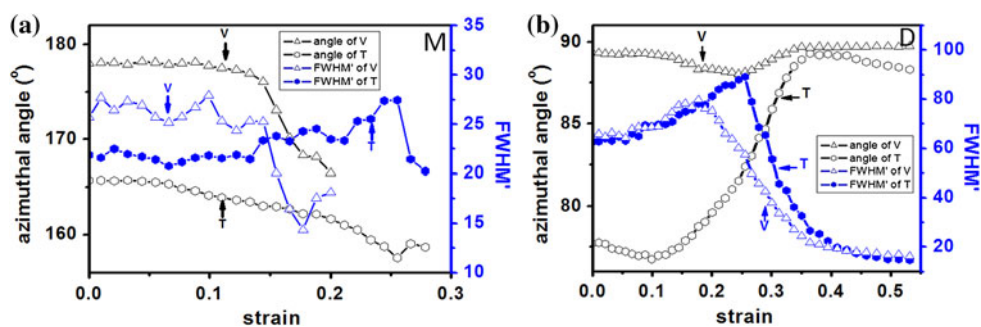


Fig. 7 The azimuthal angle and FWHM' of parent crystal (a) and daughter crystal (b) for V (vertical) and T (tilt) directions



mesophase locates at the almost same azimuthal angle with that from L_m on 2D-scattering patterns, so it is hard to evaluate the disappearance of L_m accurately. However, the scattering from L_d still can be detected clearly in the image at strain of 0.3, where mesophase emerges. For a detailed comparison, we come to the azimuthal integrated intensity of (110) which is displayed in Fig. 6a. After a tiny peak shift of L_m , two sharp peaks appear at the azimuthal angle of 90° and 270° , which are the scattering from mesophase. Meanwhile, the scattering peak of L_d keeps its position, although FWHM' becomes wider. Obviously, no matter what the drawing direction is, L_m is easier to be destroyed.

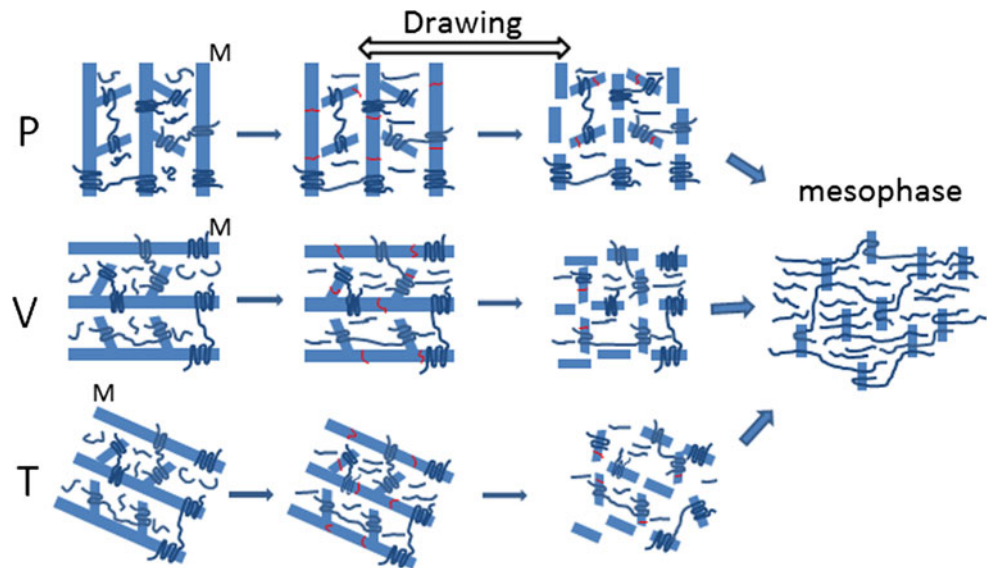
Deformation cuts large crystal into small cluster, which forms the new phase of mesophase. At mesoscopic level, the unique cross-hatched structure matches the essential requirement of auxetic material, which is hinge-like structure. In model of the cross-hatched structure, L_m plays the role of frame while L_d looks like purlines. As the external force applied on, the frame structure will sustain large part of the load, which leads to the mass destruction of L_m . Simultaneously, the L_d are damaged partially as purlines taking part of the load. After L_m are destroyed into small grains, the load is applied on L_d totally. With further stretching, the cross-hatched structure is destroyed thoroughly. After the L_m are destroyed under uniaxial drawing, the mesophase forms at such a small strain subsequently. In the research of deformation induced structure evolution of iPP, mesophase always appears at higher strain up to 1 or drawing ratio in fiber or film stretching at room temperature [30, 31]. The mesophase is pointed out to be conformationally disordered crystal and consist of small crystals of α form or β form [40]. Also, it is thought to be composed of much more disordered bundles of chains [41]. Anyway, mesophase is formed due to deformation induced structure evolution of highly oriented crystal in conventional research. In this study, the cross-hatched structure is already highly oriented before deformation. No matter what the drawing direction is, the molecular chain in L_m and L_d cannot reorient too much. Massive slip is easy to take place under deformation, which leaves small crystal clusters. The breakdown of the cross-hatched structure leads to formation of mesophase with low orientation at

such a small strain. Therefore, the process seems to be deformation cuts large crystal into small cluster, which is the origin of the new phase of mesophase.

Combining with the force conditions, it is easier to explain the shift of d-spacing as mentioned above, which also confirms the structure evolution further. According to the relation between real and reciprocal space in X-ray scattering, the force condition of (110) crystal faces for both L_m and L_d in three directions are displayed in the right column of Fig. 5. Take P experiment for example, the tensile direction is normal to the stacking of the daughter (110) faces, as shown in Fig. 5d. In the stage of elastic deformation, the crystallographic planes will be pulled away from each other as the amorphous being stretched, so the d-spacing increases from 0.623 to 0.635 nm. Due to the fine slip and rotation of crystal, the d-space recovers partially after yield strain and then keeps a plateau. Oppositely, the normal of parent (110) is perpendicular to the drawing direction, so it will be the effect of shear force which decreases the d-spacing to 0.62 nm. After yielding, the d-spacing increases continuously. In the deformation theory of Strobl and coauthors [36], a retracting force is generated to make the system tend to recover an isotropic state of optimized entropy, which is the main reason for the recovery after yielding. For the experiments of V and T, although the evolution trend of d-spacing is opposite to P experiment, it will not go into detail as the physical mechanism is same. Due to the collective activity of slip motion and destruction of crystal blocks with further deformation, it is noticed the continuous increase of parent d-spacing after recovery in Fig. 5d–f, which also confirms the damage of L_m is earlier than L_d .

According to the analysis above, Fig. 8 shows the structural evolution during deformation. (i) For P direction, the drawing direction is parallel to the interested axis of L_m . In the initial stage, L_m adjust its position and orient along external force, which can be estimated based on the change of FWHM' in Fig. 6b. Inevitably, little part of crystal will be broken under deformation, as the crystallinity is declining. Meanwhile, the increase of d-spacing indicates fine slip happens to L_m , as we can see obvious peak shift of (110), (040), and (130) from Fig. 4b. The following status

Fig. 8 Schematic deformation behavior of the cross-hatched structure in three directions *P*, *V*, and *T*, respectively



is large scale fragmentation happens to L_m which cannot reorient in drawing direction any more. The clusters with short-scale ordering make up the mesophase. (ii) For *V* experiment, the interested axis of L_m is almost perpendicular to drawing direction. Similarly, the peak shift to small angle in Fig. 4c indicates inter or intralamellar slip occurs to L_m . Before yield strain, the FWHM' of azimuthal integrated intensity from L_d increases slightly, while the azimuthal angle does not show obvious change, which means small slip happened. After yielding, the monotonous decline of FWHM' indicates further orientation of L_d in drawing direction, while L_m is destroyed as scattering from L_m fade away. At larger strain, mesophase forms basing on the crystal fragment. (iii) For *T* experiment, the interested axes of both parent and daughter lamellae are slant with respect to the drawing direction. Therefore, both kinds of lamellae are easy to rotate under deformation which can be proved by the azimuthal angle change in Fig. 7a, b, respectively. Also, slip happens to L_m as we can see obvious peak shift in Fig. 4e. However, the diffraction peaks from L_d do not shift during the stretching (Fig. 4f). In the beginning, only L_m are destroyed, while the L_d only rotate to orient in drawing direction. With further deformation, massive slip also happens to L_d , when mesophase forms based on the crystal cluster.

Conclusion

The cross-hatched structure was extensively investigated by tensile deformation from multidirections with in situ synchrotron radiation WAXS. The cross-hatched structure, which influence the material performance extensively, is difficult to be studied from aspect of mechanical property

due to the structural similarity of L_m and L_d . We successfully developed the method to preorient iPP sample which ensure the study of the structure evolution of L_m and L_d separately with in situ environments. Thank to this method, it is fancy to find that L_m is destroyed earlier than L_d , which can be attributed to the former one plays the role of frame during deformation in this work. The deformation behaviors from three directions are discussed, and the corresponding model is presented. As the sample has been preoriented, massive slip occurs easily which lead to fragment of crystal. Therefore, mesophase appears much earlier than conventional study. Also, the close relationship between deformation induced mesophase and cross-hatched structure is found in the study.

Acknowledgements This study is supported by the National Natural Science Foundation of China (51033004, 50973103, 51120135002), 973 program of MOST (2010CB934504). The research is also in part supported by “the Fundamental Research Funds for the Central Universities”.

References

1. Norton DR, Keller A (1984) On the morphology of blends of linear and branched polyethylene. *J Mater Sci* 19:447–456
2. Padden FJ, Keith HD (1959) Spherulitic crystallization in polypropylene. *J Appl Phys* 30:1479–1484
3. Natta G, Peraldo M, Corradini P (1959) Smectic mesomorphic form of isotactic polypropylene. *Rend Accad Naz Lincei* 26:14–17
4. Corradini P, Petraccone V, Derosa C, Guerra G (1986) On the structure of the quenched mesomorphic phase of isotactic polypropylene. *Macromolecules* 19:2699–2703
5. Samuels RJ, Yee RY (1972) Characterization of structure and organization of beta-form crystals in type-iii and type-iv beta-isotactic polypropylene spherulites. *J Polym Sci* 10:385–432

6. Natta G, Ganis P (1960) Structure and properties of isotactic polypropylene *Nuovo Cimento Series X*:40–51
7. Bruckner S, Meille SV, Petraccone V, Pirozzi B (1991) Polymorphism in isotactic polypropylene. *Prog Polym Sci* 16:361–404
8. Somani RH, Hsiao BS, Nogales A et al (2000) Structure development during shear flow-induced crystallization of i-pp in-situ small-angle X-ray scattering study. *Macromolecules* 33:9385–9394
9. Schneider K (2010) Investigation of structural changes in semicrystalline polymers during deformation by synchrotron X-ray scattering. *J Polym Sci Part B* 48:1574–1586
10. Somani RH, Hsiao BS, Nogales A, Fruitwala H, Srinivas S, Tsou AH (2001) Structure development during shear flow induced crystallization of i-pp in situ wide-angle X-ray diffraction study. *Macromolecules* 34:5902–5909
11. Bruckner S, Meille SV (1989) Non-parallel chains in crystalline gamma-isotactic polypropylene. *Nature* 340:455–457
12. Lotz B, Wittmann JC (1986) The molecular-origin of lamellar branching in the alpha-(monoclinic) form of isotactic polypropylene. *J Polym Sci Part B* 24:1541–1558
13. Khoury F (1966) Spherulitic crystallization of isotactic polypropylene from solution—on evolution of monoclinic spherulites from dendritic chain-folded crystal precursors. *J Res Natl Bur Std A* 70:29–61
14. Padden FJ, Keith HD (1966) Crystallization in thin films of isotactic polypropylene. *J Appl Phys* 37:4013–4020
15. Lovinger AJ (1983) Microstructure and unit-cell orientation in alpha-polypropylene. *J Polym Sci Polym Phys* 21:97–110
16. Binsberg FL, Delange BGM (1968) Morphology of polypropylene crystallized from melt. *Polymer* 9:23–40
17. Lotz B, Wittmann JC, Lovinger AJ (1996) Structure and morphology of poly (propylenes): a molecular analysis. *Polymer* 37:4979–4992
18. Clark ES, Spruiell JE (1976) Unlimited flex life in molded-in hinge in polypropylene—structural hypothesis. *Polym Eng Sci* 16:176–181
19. Phillips A, Zhu PW, Edward G (2006) Simple shear deformation of polypropylene via the equal channel angular extrusion process. *Macromolecules* 39:5796–5803
20. Zhu PW, Tung J, Edward G, Nichols L (2008) Effects of different colorants on morphological development of sheared isotactic polypropylene: a study using synchrotron wide-angle X-ray scattering. *J Appl Phys* 103:124906–124907
21. Pang YY, Dong X, Liu KP, Han CC, Chen EQ, Wang DJ (2008) Ductile-brittle transition controlled by isothermal crystallization of isotactic polypropylene and its blend with poly (ethylene-co-octene). *Polymer* 49:4259–4270
22. Aboulfaraj M, Gsell C, Ulrich B, Dahoun A (1995) In-situ observation of the plastic-deformation of polypropylene spherulites under uniaxial tension and simple shear in the scanning electron-microscope. *Polymer* 36:731–742
23. Flory PJ, Yoon DY (1978) Molecular morphology in semi-crystalline polymers. *Nature* 272:226–229
24. Peterlin A (1971) Molecular model of drawing polyethylene and polypropylene. *J Mater Sci* 6:490–508
25. Bowden PB, Young RJ (1974) Deformation mechanisms in crystalline polymers. *J Mater Sci* 9:2034–2051
26. Lin L, Argon AS (1994) Structure and plastic-deformation of polyethylene. *J Mater Sci* 29:294–323
27. Peterlin A (1987) Drawing and extrusion of semicrystalline polymers. *Colloid Polym Sci* 265:357–382
28. Wignall GD, Wu W (1983) A sans investigation into the role of melting and recrystallization during solid-state deformation of polyethylene. *Polymer Comm* 24:354–359
29. Zia Q, Radusch H-J, Androsch R (2009) Deformation behavior of isotactic polypropylene crystallized via a mesophase. *Polym Bull* 63:755–771
30. Ran SF, Zong XH, Fang DF, Hsiao BS, Chu B, Phillips RA (2001) Structural and morphological studies of isotactic polypropylene fibers during heat/draw deformation by in-situ synchrotron saxs/waxd. *Macromolecules* 34:2569–2578
31. Ran SF, Zong XH, Fang DF et al (2001) Studies of the mesophase development in polymeric fibers during deformation by synchrotron saxs/waxd. *J Mater Sci* 36:3071–3077
32. Hay IL, Keller A (1965) Polymer deformation in terms of spherulites. *Kolloid-Zeitschrift Zeitschrift Fur Polymere* 204:43–74
33. Zuo F, Keum JK, Chen XM et al (2007) The role of interlamellar chain entanglement in deformation-induced structure changes during uniaxial stretching of isotactic polypropylene. *Polymer* 48:6867–6880
34. Nozue Y, Shinohara Y, Ogawa Y et al (2007) Deformation behavior of isotactic polypropylene spherulite during hot drawing investigated by simultaneous microbeam saxs-waxs and pom measurement. *Macromolecules* 40:2036–2045
35. Hammersley AP (2004) fit2d-v10.3 <http://www.esrf.fr/computing/scientific/FIT2D/>. Accessed 28 Dec 2013
36. Men YF, Rieger J, Strobl G (2003) Role of the entangled amorphous network in tensile deformation of semicrystalline polymers. *Phys Rev Lett* 91:095502
37. Meijer HEH, Govaert LE (2005) Mechanical performance of polymer systems: the relation between structure and properties. *Prog Polym Sci* 30:915–938
38. van Melick HGH, Govaert LE, Meijer HEH (2003) On the origin of strain hardening in glassy polymers. *Polymer* 44:2493–2502
39. Galeski A (2003) Strength and toughness of crystalline polymer systems. *Prog Polym Sci* 28:1643–1699
40. Kang YA, Kim KH, Ikehata S et al (2011) In-situ analysis of fiber structure development for isotactic polypropylene. *Polymer* 52:2044–2050
41. Qiu J, Wang ZG, Yang L, Zhao JC, Niu YH, Hsiao BS (2007) Deformation-induced highly oriented and stable mesomorphic phase in quenched isotactic polypropylene. *Polymer* 48:6934–6947